King Saud University

Journal of King Saud University – Science

www.ksu.edu.sa
www.sciencedirect.com

ORIGINAL ARTICLE

Investigation on the key features of L-Histidinium 2-nitrobenzoate (LH2NB) for optoelectronic applications: A comparative study

CrossMark

Mohd. Shkir *

Department of Physics, Faculty of Science, King Khalid University, P.O. Box 9004, Abha 61413, Saudi Arabia

Abstract The current work is to highlight the fundamental acumen about the molecular structure, photophysical and static first hyperpolarizability (β) of L-Histidinium 2-nitrobenzoate (LH2NB) organic molecule for the first time. Hartree–Fock (HF) and density functional theory (DFT) has been applied using different functional at 6-31G** basis set for the first time. The strong correlation has been observed between experimental and theoretical vibrational spectra. TD-DFT method has been used at different levels of theory to study the UV–Visible spectra. The analysis of HOMO and LUMO was done to explain the charge interaction taking place within the molecule and the energy gap was evaluated. The value of dipole moment is found to be lower in excited state than ground state as calculated from all applied methods. The value of total static first hyperpolarizability was found to be 7.447×10^{-30} esu at B3LYP/6-31G** level of theory, which is about 20 times higher than urea molecule. The current results indicate that the studied molecule may be a decent applicant for opto-electronic applications.

1. Introduction

Since last few decades the research and development on L-Histidine and its complexes has been receiving an immense attention due to their easy synthesis, growth and good nonlinear optical (NLO) properties and hence emerges as one of the most extensively explored amino acid from its family. It can forms a variety of complexes with different organic and inorganic materials such as: gold (III)–L-histidine (Cuadrado et al., 2000), L-Histidinium 2-nitrobenzoate (Moovendaran et al., 2013; Natarajan et al., 2012), l-histidine-4-nitrophenolate 4-nitrophenol (LHPP) Dhanalakshmi et al., 2010, l-histidine acetate (Madhavan et al., 2007), L-Histidinium perchlorate (LHPCL) Aruna et al., 2007, l-Histidine nitrate (Dhas and Natarajan, 2008), L-histidinium trifluoroacetate (Dhas et al., 2008), l-histidine hydrofluoride dihydrate (LHHF) Madhavan et al., 2006, l-histidine hydrochloride monohydrate (Anandan and Jayavel, 2011; Madhavan et al., 2007), and l-histidine

* Address: Department of Physics, College of Science, King Khalid University, Saudi Arabia. Tel.: +966 530683673; fax: +966 72418319.
E-mail addresses: shkirphysics@gmail.com, shkirphysics@kku.edu.sa.
Peer review under responsibility of King Saud University.

ELSEVIER **Production and hosting by Elsevier**

bromide (Ahmed et al., 2008) and shows noticeable Second Harmonic Generation (SHG) efficiency. L-Histidine has another important advantage of being an organic material, which is well known due to its low cost, extraordinary nonlinearity, high optical threshold, synthetic litheness, and easy molecular design. Also its configuration can be modified to get the desired nonlinear optical (NLO) properties for tailor made applications and also shows low dielectric constants which makes it useful in terahertz (THz) generation devices (Boomadevi et al., 2004; Moovendaran et al., 2012; Zyss et al., 1984; Chemla, 2012; Shakir et al., 2010, 2014; Ledoux et al., 1987; Fujiwara et al., 2006; Shakir et al., 2009).

The synthesis of a new L-Histidine compound named L-Histidinium 2-nitrobenzoate (LH2NB) (chemical structure shows in Fig. 1) has been reported (Natarajan et al., 2012), and its crystallization, molecular structure, vibrational, optical, second harmonic generation (SHG) efficiency and thermal properties are described. Moovendaran et al. (2013) has reported the SHG efficiency of titled compound which is about 2 times higher than standard KDP crystal.

As per the current available literature it is clear that only experimental studies have been performed on the titled compound so far. However, it is very important and justified to study its theoretical properties such as geometrical, vibrational, photophysical, nonlinear etc. using HF and density functional theory (DFT) to understand the mechanism responsible for its use in various optoelectronic applications. Hartree–Fock (HF) and DFT show key advantages in calculating the various parameters such as: vibrational frequencies, molecular geometries of different kinds of materials very precisely within short time and at low cost (Johnson et al., 1993; Cinar et al., 2014; Shkir and Abbas, 2014a, 2014b; Arivazhagan and Meenakshi, 2012; Reshak and Khan, 2014; Govindarasu and Kavitha, 2014; Elleuch et al., 2007; Shkir et al., 2014, 2015a, 2015b, 2015c, 2015d). Furthermore, the range separated functionals such as CAM-B3LYP, wb97xd and many more are efficient to calculate the electronic and nonlinear optical (NLO) properties which are much superior to the conventional methods (Johnson et al., 1993; Cinar et al., 2014; Shkir and Abbas, 2014a, 2014b; Arivazhagan and Meenakshi, 2012; Reshak and Khan, 2014; Govindarasu and Kavitha, 2014; Elleuch et al., 2007; Shkir et al., 2014, 2015a, 2015b, 2015c; Abbas et al., 2015).

In the current work, the author's goal is to highlight the key features of LH2NB molecule by HF and DFT (using different functional) studies carried out for the first time. It may be noted here that the reason for applying the different functional is to have a in-depth knowledge about the appropriateness of functional which gives better results for the titled molecule as every functional has different extension of DFT.
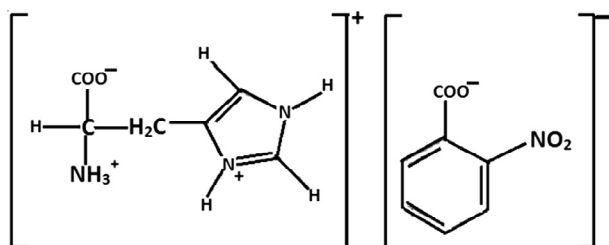

Figure 1 Chemical structure of LH2NB.

2. Computational details

HF (Fischer et al., 1973) and DFT using B3LYP- Becke's three parameter exchange functional B3 combined with Lee–Yang-Parr correlation functional LYP (Becke, 1993; Lee et al., 1988) for obtaining the molecular structures, IR and Raman spectra. Further the TD-DFT study has been performed using B3LYP along with range separated functional such as CAM-B3LYP (Yanai et al., 2004), wb97xd (Chai and Head-Gordon, 2008), PBE0 (Adamo and Barone, 1999), M06 (Zhao and Truhlar, 2008) for calculating opto-electronic properties (Dreuw and Head-Gordon, 2004; Foster and Wong, 2012; Wong et al., 2009; Gibbs et al., 2011). The stable geometry was achieved following the true minimum on the potential energy surface (PES) attained by solving the self-consistent field equation. Infrared (IR) and vibrational (Raman) frequencies were calculated using optimized structural parameters to characterize all stationary points as minima. All the theoretical calculations were made using Gaussian 09W program package (Frisch et al., 2009) with the default convergence principles, without any constraint on the geometry. By applying the different functional the dipole moment, polarizability, anisotropy of polarizability, and static and total first hyperpolarizability values were calculated. Finite Field (FF) method was employed to calculate the value of total first hyperpolarizability (β_{tot}) and its tensor components. FF method was generally applied to know the nonlinear optical properties because this approach can be used in concert with the electronic structure method to work out β values. β_{tot} values calculated by this method is found to be genuine with experimental structure property relationship recently. A static electric field (F) has been applied to a molecule in FF method and the energy (E) is expressed by the following relation:

$$E = E^{(0)} - \mu_1 F_1 - \frac{1}{2}\alpha_{ij}F_iF_j - \frac{1}{6}\beta_{ijk}F_iF_jF_k - \frac{1}{24}\gamma_{ijkl}F_iF_jF_kF_l - \ldots \tag{1}$$

where $E^{(0)}$ is the energy of molecule in the absence of an electric field, μ is components of the dipole moment vector, α is the linear polarizability tensor, β and γ are the first and second hyperpolarizability tensors respectively, while i,j and k label the x,y and z components respectively. Values of μ, α, β, and γ can be obtained by differentiating Eq. (1) with respect to F.

The value of static hyperpolarizability (β_0) can be calculated from the following equation:

$$\beta_0 = \frac{3}{5}\beta_{tot} \tag{2}$$

Further, the optical absorption spectra were calculated by time dependent DFT (TDDFT) study suing different functional.

GCRD parameters of the titled molecule have been calculated as follows:

A relation for absolute hardness (η) was established Parr and Chattaraj, 1991; Pearson, 1985; Parr and Pearson, 1983 i.e.:

$$\eta = \frac{I - A}{2} \tag{3}$$

where I is the vertical ionization potential energy and A is vertical electron affinity.

Koopman's theorem is associated within the structure of HF self-consistent field molecular orbital theory (Koopmans, 1933), the ionization energy and electron affinity can be specified over HOMO and LUMO orbital energies as given below:

$$I = -E_{HOMO} \quad \text{and} \quad A = -E_{LUMO}$$

I and A values of LH2NB molecule are presented in Table 5. Greater HOMO energy is related to the more reactive molecule in the reactions with electrophile, while minor LUMO energy is necessary for molecular reactions with nucleophile (Rauk, 2001). The hardness of any molecule is related to the HOMO–LUMO energy gap and expressed as.

$$\eta = \frac{1}{2}(E_{LUMO} - E_{HOMO}) \tag{4}$$

Electronic chemical potential is achieved by:

$$\mu = -\left(\frac{I + A}{2}\right) \tag{5}$$

Chemical softness is achieved by:

$$S = \frac{I}{2\eta} \tag{6}$$

Electronegativity is achieved by:

$$\chi = \left(\frac{I + A}{2}\right) \tag{7}$$

The electrophilicity index is achieved by:

$$\omega = \frac{\mu^2}{2\eta} \tag{8}$$

3. Results and discussion

3.1. Molecular geometry

The stable molecular geometry of LH2NB was achieved by HF and B3LYP using 6-31G** basis set as shown in Fig. 2 (a) and (b) respectively. The coordinates used in the current work for theoretical calculations were earlier reported CCDC-857702 (Natarajan et al., 2012). The geometry was also optimized by other methods such as B3LYP, CAM-B3LYP and wb97xd levels of theory using 6-31G** basis set. Some important geometrical parameters such as bond lengths, bond angles are tabulated in Table 1 calculated by HF and B3LYP and compared with experimental values (Natarajan et al., 2012) and found in good relationship. The hydrogen bonding is denoted by peppered line and the values of these hydrogen bonds are given in Table 2 obtained at all levels of theory. As clear from Table 2 the geometry optimized by HF is found to be in better agreement than other methods with experimental (Natarajan et al., 2012).

Therefore, here author focused on geometrical parameters obtained from the HF method, as clear from figure (Fig. 2) that several hydrogen bondings have been observed between L-Histidinium (act as cation) and p-nitrobenzoic acid (act as anion). Three intermolecular hydrogen bondings such as the first one between H(17) and O(35) atoms i.e. N(12)–H(17)—O(35) [H(17)—O(35) = 1.7215 Å], second between H(20) and O(34) atoms i.e. N(14)–H(20)—O(34) [H(20)—O(34) = 1.6902 Å], and third one between H(11) and O(36) atoms

i.e. C(10)–H(11)—O(36) [H(11)—O(36) = 2.6428 Å] have been observed. Three intramolecular hydrogen bondings were observed in L-histidine molecule itself between N(12) and (H (18) atoms i.e. N(12)–H(18)—O(15) [H(18)—O(15) = 2.9384 Å], N(12) and H(19) atoms i.e. N(12)–H(19)—O (15) [H(19)—O(15) = 1.9553 Å] and H(9) and O(16) atoms i.e. C(8)–H(9)—O(16) [H(9)—O(16) = 2.6788 Å], respectively. The bondings observed by HF as well as by other methods are given in Table 2 along with experimentally reported values (Natarajan et al., 2012) and it shows that molecular geometry obtained by HF is in good agreement than other methods. It may be mentioned here that by other applied methods only four bondings were observed. Because of a large number of hydrogen bondings and charge transfer in the titled molecule it is expected that it will show great NLO properties (Cole et al., 2001). The reason for the difference in bond lengths and angles is that the experimental values were obtained from the X-ray diffraction of the crystalline material in solid crystal form, though the geometry optimization of LH2NB was performed for an isolated molecule. The lowest value of C_7–C_8 (1.343 Å) less than the standard value (1.54 Å) of C–C bond length was observed. Correspondingly, the calculated shortest value for C–O bond length comes out to be 1.222 Å, which is less than the standard value (1.43 Å) of C–O bond length. The other bond lengths such as C–C, C–O, C–N, N–O, and C–H etc. in LH2NB are inside the range of typical values. The bond lengths of C–H are remain between 1.091 Å and 1.10 Å (Shkir and Abbas, 2014b).

3.2. Vibrational analysis

It is well known in the literature that the vibrational (Infrared and Raman) spectroscopic techniques have been widely applied by the organic chemists to study the functional groups, bonding to different molecular conformations and reaction mechanisms by tentatively assigning their observed fundamental modes (Teimouri et al., 2009; Colthup, 2012; Socrates, 2004; Dollish et al., 1974; Smith, 1998; Roeges, 1994). It is well known that when hydrogen (H), nitrogen (N), oxygen (O) etc. atoms are present between two molecules or within a molecule the inter-molecular and intra-molecular hydrogen bonding appears. The calculated IR and Raman spectra of LH2NB using HF and B3LYP methods are shown in Fig. 3. The theoretically calculated frequencies can be well matched with the experimentally observed frequencies by applying the scaling factor (for HF, 0.8929 and B3LYP, 0.9613) (Sinha et al., 2004; Alcolea Palafox, 2000; Shkir et al., 2015). IR and Raman frequencies of various theoretically predicted and experimentally observed peaks with their tentative assignment are listed in Table 3 and comparison exhibits strong agreement with the reported values.

The vibrational modes present in the molecule at ~3177, 3187 cm^{-1} in HF and B3LYP respectively, are due to NH symmetric stretching vibration. In the similar manner the band observed at 3105, 3113 cm^{-1}, and 3153 cm^{-1} have been tentatively assigned to NH_3 stretching vibration mode. The CH_2, NH_3 symmetric stretching vibrations are observed in the region of 2800–3001 cm^{-1}. The band at 2478, 2470 cm^{-1} observed in Raman not in IR may be assigned to C–H combinational overtone. The COO^- ions of carboxylic group shows asymmetric and symmetric stretching characteristic modes at
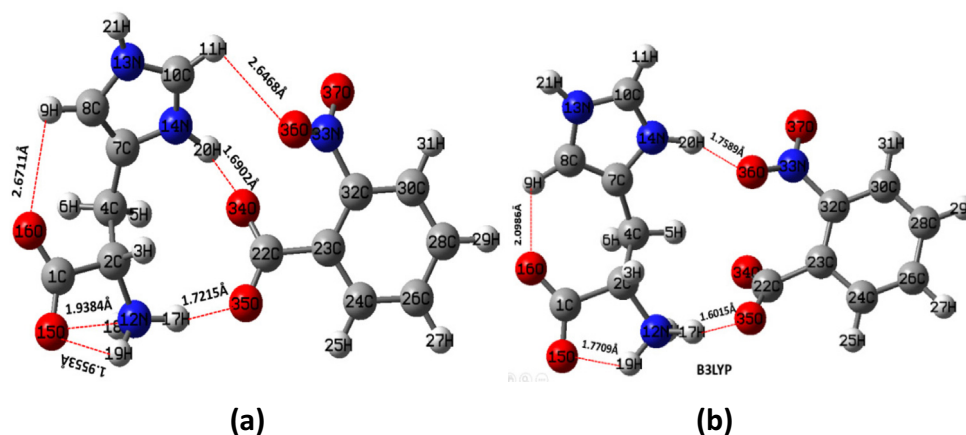
Figure 2 Optimized stable molecular geometry of LH2NB by (a) HF and (b) B3LYP using 6-31G** basis set.

1650, 1634, 1639 cm^{-1} and 1433, 1440 cm^{-1} in IR and Raman respectively. COO^{-} bending and wagging vibration modes were observed at 815, 799 cm^{-1} and 823, 808 cm^{-1} in IR transmittance and Raman spectra respectively. The band observed at 1393, 1361 cm^{-1} and 1353 cm^{-1} have been assigned to CH$_2$ deformation. The asymmetric and symmetric stretching modes of NO$_2$ functional group is expected in the region of 1370–1330 cm^{-1} and observed at 1361, 1313 cm^{-1} and 1330, 1336 cm^{-1} in these IR transmittance and Raman spectra respectively. The wagging and rocking modes of vibration of NO$_2$ group are observed at 694 cm^{-1} and 690 cm^{-1}. The other vibration modes observed in LH2NB molecule are tentatively assigned in Table 3 which exhibits very well correlation between theoretically calculated and experimentally observed peaks in their respective IR and Raman spectra.

3.3. Optical (TD-DFT) study

Time dependent DFT (TD-DFT) is one of the broad approaches in quantum chemistry as well as in solid state physics to calculate the excited state electronic structure. The contemporary DFT methods display a promising stability between accuracy and computational efficiency, when equated to the traditional ab initio and semi-empirical approaches. To examine the kind of electronic transition in LH2NB molecule in gas phase, the TD-DFT has been applied at different functional. As almost precise absorption wavelength can be easily detected at relatively small computing time by such study on the basis of optimized ground state geometry, which is related to the vertical electronic transitions (Kostova et al., 2010; Jacquemin et al., 2005, 2004; Cossi and Barone, 2001). The UV-Vis spectrum was also calculated for the optimized geometry at TD-HF level of theory using 6-31G** basis set as shown in Figure 1S (see supplementary data). Absorption wavelength, excitation energies, oscillator strengths and dipole moments were evaluated at the ground state of the optimized geometries using TD-B3LYP, TD-CAM-B3LYP, TD-wb97xd, TD-PBE0, TD-M06 levels of theory using 6-31G** basis set. These calculated values are presented in Tables 4 and 5. The calculated UV–Vis spectrum of LH2NB has only one absorption band at all applied functional as shown in Fig. 4. The value of excitation wavelength is found to be ∼328.19 (3.778 eV), 309.07 (4.012 eV), 310.64 (3.990 eV) nm, 317 (3.935 eV) nm and 324

(3.820 eV) nm calculated at B3LYP, CAM-B3LYP, wb97xd, PBE0 and MO6 levels of theory using 6-31G** basis set, respectively. The oscillatory strength describes the strength of optical or molecular interactions. The value of f for the titled molecule is found to be between 0.02 to 0.05 obtained at all applied methods. The value of f is used to compare a quantum mechanical transition to that expected by a fully allowed set of classical electromagnetic oscillators. The value of $f = \sim 1$, represents a strong transition while generally a quantum mechanically forbidden transition may have $f = \sim 0.001$. It may be mentioned here that the optimized coordinate at B3LYP has been used in PBE0 and MO6. In experimentally reported result on optical transmission there is a absorption band at about 300 nm (Moovendaran et al., 2013), which is in good agreement with the theoretical value calculated at almost all levels of theory, however it is more close to CAM-B3LYP. The present study reveals that the titled compound owns the property of extended ultraviolet–visible transmittance (Govindarajan et al., 2011; Srinivasan et al., 2006). The obtained high excitations energy (or optical absorption spectra which help us to determine the optical transparency and band gap of the materials) is maybe useful in various optoelectronic devices (Shkir et al., 2014; Kushwaha et al., 2011; Shakir et al., 2009; Kushwaha et al., 2014). The optical band gap was calculated by using Tauc's relation from the absorption spectra obtained from B3LYP and found to be about 3.3 eV. This shows that the titled material possesses high band gap in comparison to other optical materials as well as comparable (Shkir et al., 2014; Babu et al., 2010; Klimm, 2014) and can be used in optical devices. The change in the dipole moment (Table 5) upon excitation was observed which may be due to charge redistribution within HOMO and LUMO orbitals of LH2NB molecule. The titled molecule has less polar excited state than the ground state as the value of dipole moment is higher in the ground state.

3.4. HOMO–LUMO gap and GCRD analysis

It is very important to study the frontier molecular orbitals (FMOs) as they play a significant character in the reactivity of any molecule. The interactions of HOMO and LUMO in reacting species throughout the progression of chemical reactions are essential among FMOs in stabilization of transition

Table 1 The bond lengths [Å], bond angles [°] of LH2NB molecule optimized molecule at HF and B3LYP levels of theory.

Bond lengths (Å)				Bond Angles (°)							
Bonds	Exp. (Natarajan et al., 2012)	HF	B3LYP	Bonds	Exp. (Natarajan et al., 2012)	HF	B3LYP	Bonds	Exp. (Natarajan et al., 2012)	HF	B3LYP
C1–O15	1.224(2)	1.229	2.256	O15–C1–O16	126.5(2)	132.676	130.927	C23–C24–C26	122.2(2)	121.335	121.318
C1–O16	1.266(2)	1.222	1.248	O15–C1–C2	118.0(2)	113.140	113.147	C28–C26–C24	119.7(2)	120.292	120.553
C1–C2	1.530(2)	1.561	1.581	O16–C1–C2	115.5(2)	114.180	115.926	C30–C28–C26	119.7(2)	119.672	119.583
C2–N12	1.483(2)	1.489	1.497	N12–C2–C1	110.7(1)	107.873	105.962	C28–C30–C32	119.8(2)	118.873	118.756
C2–C4	1.533(2)	1.531	1.539	N12–C2–C4	107.8(1)	111.983	111.456	C30–C32–C23	122.2(2)	122.983	123.129
C4–C7	1.485(3)	1.494	1.495	C1–C2–C4	110.2(2)	113.374	114.156	C30–C32–N33	117.7(2)	115.461	116.628
C7–C8	1.354(3)	1.343	1.370	C7–C4–C2	112.2(2)	110.260	113.151	C23–C32–N33	120.1(2)	121.492	120.175
C7–N14	1.371(3)	1.379	1.388	C8–C7–N14	106.3(2)	106.559	106.153	C10–N13–C8	108.7(2)	109.168	109.883
C8–N13	1.370(3)	1.384	1.383	C8–C7–C4	132.3(2)	132.954	131.590	C10–N14–C7	109.1(2)	109.806	110.163
C10–N13	1.316(3)	1.320	1.341	N14–C7–C4	121.4(2)	120.339	122.256	O36–N33–O37	123.5(2)	124.252	123.343
C10–N14	1.321(3)	1.303	1.332	C7–C8–N13	107.3(2)	106.307	106.596	O36–N33–C32	117.9(2)	117.756	116.947
C22–O34	1.234(3)	1.239	1.252	N13–C10–N14	108.7(2)	108.150	107.202	O37–N33–C32	118.6(2)	117.883	119.630
C22–O35	1.253(2)	1.232	1.265	O34–C22–O35	126.9(2)	127.414	128.482				
C22–C23	1.523(3)	1.522	1.529	O34–C22–C23	116.9(2)	116.333	115.621				
C32–N33	1.459(2)	1.462	1.458	O35–C22–C23	115.9(2)	116.195	115.833				
N33–O37	1.221(3)	1.188	1.225	C24–C23–C22	116.6(2)	119.005	119.570				
N33–O36	1.218(3)	1.199	1.245	C32–C23–C22	127.0(2)	123.946	123.387				

Table 2 Main possible hydrogen bond in LH2N molecule (Å) obtained different levels of theory using 6–31G** basis set.

Bond (H—A)	Exp. (Natarajan et al. 2012)	HF	B3LYP	CAM-B3LYP	wb97xd
17H—35O	2.18	1.7215	1.6015	1.5743	1.6140
20H—34O	1.88	1.6902	1.7589	1.7519	1.7490
11H—36O	2.36	2.6468	–	–	–
19H—15O	1.97	1.9553	1.7709	1.7451	1.7560
18H—15O	1.84	2.9384	–	–	–
9H—16O	2.41	2.6788	2.0986	2.0722	2.0744

structure. Chemical reactivity, kinetic stability, optical polarizability and chemical softness can be described by HOMO–LUMO energy gap values of any molecular system. It is well known that larger the energy gap the harder the material and also shows higher thermal and kinetic stability according to softness–hardness rule. The energy values of HOMO and LUMO orbitals calculated by the B3LYP method are found to be −5.442 and −2.748 eV, respectively. The value of HOMO–LUMO gap is 2.694 eV with chemical hardness 1.347 eV, indicates that the titled material has good chemical stability.

TD-DFT results revealed the excitation energy about 3.778, 3.836 and 3.990 eV calculated by B3LYP, CAM-B3LYP, wb97xd, PBE0/PBE1PBE and MO6 levels of theory viz. corresponding to the electronic transition from ground state to excited state and displays that the charge transfer from L-Histidine to 2-nitrobenzoate ligand counterparts. Fig. 5 shows the 3-D plot of HOMO–LUMO orbitals and their respective values are presented in Table 6, determined at B3LYP/6-31G** level of theory. The HOMO–LUMO orbitals were also obtained at HF/6-31G** level of theory and their 3-D plot of is shown in Figure 2S (see supplementary data). From the figure it is clearly visible that the HOMO are localized at the lower part of L-Histidine and COO group of 2-nitrobenzoate molecule while LUMO are localized on 2-nitrobenzoate molecule only. LH2NB has an advantage of noteworthy transparency and low absorbance as experimentally proved (Moovendaran et al., 2013).

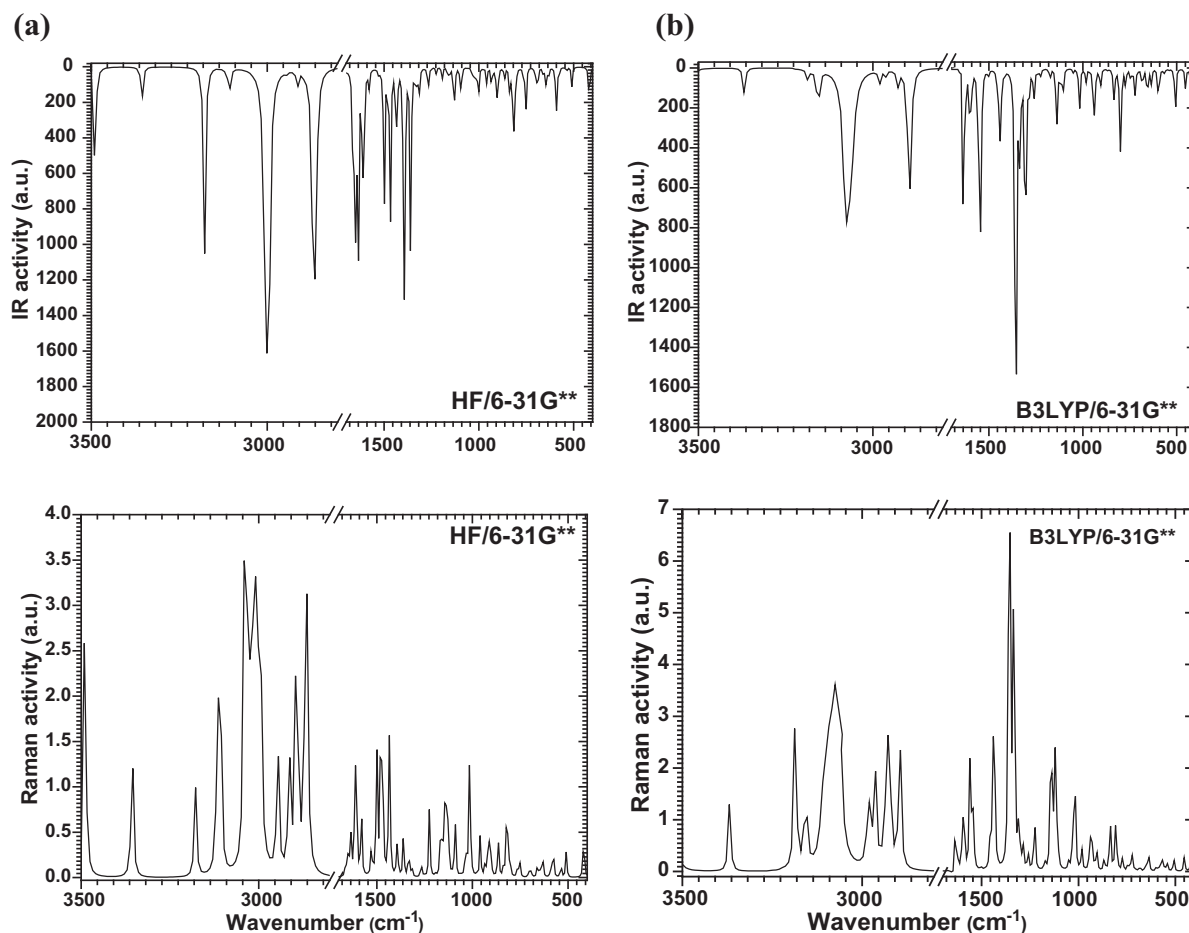Further the global chemical reactivity descriptor (GCRD) parameters were calculated as these are used to identify the

Figure 3 Calculated IR and Raman spectra of LH2NB by (a) HF and (b) B3LYP level of theory.

Table 3 HF and B3LYP calculated IR and Raman and experimentally reported IR frequencies with their appropriate assignments for LH2NB using 6-31G** basis set.

HF Calculated IR freq. (Cm^{-1})	B3LYP Calculated IR freq. (Cm^{-1})	Reported Experimental IR freq. (Cm^{-1}) (Moovendaran et al., 2013)	HF Calculated Raman freq. (Cm^{-1})	B3LYP Calculated Raman freq. (Cm^{-1})	Assignments
3354	3370	–	3355	3369	NH_3 asymmetric stretching
3177	3187	3173	3177	3187	NH symmetric stretching
3105	3153	3138	3113	3153	[NH_3] Hydrogen bonded stretching mode
3001,2912, 2864	3075,2980,2962, 2928,2893	2970,2818 –	3041,3009,2944,2912,2896,2864	3075,2962, 2928,2893	CH_2, NH_3 symmetric stretching –
–	2478	2560,2363	–	2470	C–H combinational overtone
1650,1634	1639	1639	1634	1639	COO^- asymmetric stretching
1610,1578	1604	1578	1610,1578	1595	NH_3 symmetric stretching
–	1543	1533	1530	1561	N=C–N stretching
1498	1500	1491	1498,1482	–	Ring deformation
1433	1440	1421	1433	1440	COO^- symmetric stretching
1393	1353	1377	1393,1361	1353	CH_2 deformation
1361,1313 –	1336 –	1348 –	1330 –	1336 –	NO_2 symmetric stretching + C–C stretching
1265	1301	1288	1265	1310sh,1284	C–C stretching + C=O stretching
1225	1258,1223	1258	1225	1258,1223	C–H in plane bending + C–O bending
1192,1160,1128	1171sh,1137	1136	1144	1172sh,1137	C–H in plane bending
1096	1050	1067	1088	1052sh	Ring breathing, C–H in plane bending
1000,959,935,903	1016,981,938,903	1001,904	1016,959,911	1016,981,938,903	N–H bending
839	834	831	860	834	C–C stretching
815	799	785	823	808	COO^- bending vibration
750	747,721	754	750	748,721	CCC in plane bending
694	690	694	694	–	NO_2 wagging
662	687	667	662	687	NO_2 rocking
646	653	652	–	–	COO^- wagging
630	634	629	630	635	Ring deformation
590	600,566	575	574	600sh,566,540	$C–NO_2$ stretching
509	505	519	509	505	COO^- wagging
421	419	422	421	419	CCC out of plane bending

connection regarding structure, stability and global chemical reactivity of any molecule. GCRD parameters are used in quantitative structure–property, structure–activity, structure–
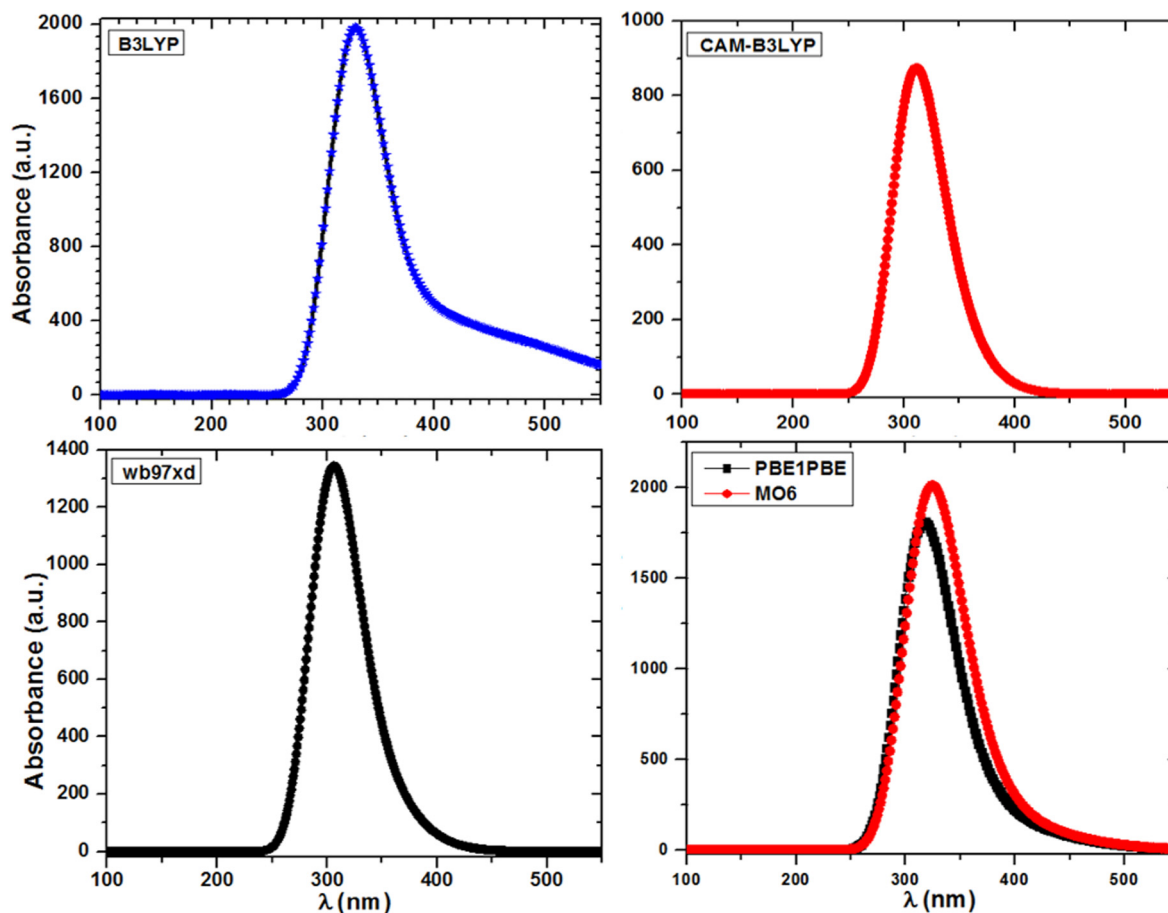
toxicity analysis and a relationship between aromaticity and hardness (Vektariene et al., 2009). DFT has been used in the present study which delivers the interpretations of important universal insights into stability and reactivity of molecular structure (Pearson, 1987). The GCRD (such as hardness (η), chemical potential (μ), softness (S), electronegativity (χ) and electrophilicity index (ω)) of LH2NB molecule have been calculated with the help of E_{HOMO} as ionization potential (I) and E_{LUMO} as electron affinity (I) respectively. The calculated values of GCRD parameters for LH2NB molecule are presented in Table 6. Thermodynamic properties were also calculated at constant temperature (298.150 K) and pressure (1.000 Atm.) as given in Table 7. The results show that the titled material has good thermal stability.

Table 4 Absorption wavelength (λ), excitation energies E(eV) and oscillator strengths (f).

Functional	λ (nm)	E (eV)	f
B3LYP	328.19	3.778	0.0450
CAM-B3LYP	309.07	4.012	0.0202
wb97xd	310.64	3.991	0.0225
PBE0	317	3.935	0.0377
M06	324	3.820	0.0386

Table 5 Total dipole moment (Debye) and its components in ground and excited state calculated at different levels of theory.

Components	HF		B3LYP		CAM-B3LYP		wb97xd	
	G.S.	E.S.	G.S.	E.S.	G.S.	E.S.	G.S.	E.S.
μ_X	−7.434	−5.732	−8.761	−3.292	−8.586	−3.329	−8.582	−3.441
μ_y	14.268	6.389	12.947	11.167	13.384	11.058	13.358	11.553
μ_z	−9.111	1.413	−8.358	−1.806	−8.447	−2.053	−8.492	−2.076
μ_{tot}	18.489	8.699	17.727	11.782	18.006	11.730	18.005	12.232

Figure 4 Calculated optical absorption spectra of LH2NB molecule at different levels of theory.

3.5. NLO (polarizability and first order hyperpolarizability) effect

The NLO processes are of technological significance in the production of laser devices, therefore in recent decade it is considered as a key subject of study, in which hyperpolarizability played a vital role and maintains the growing application and adoring to the exact determination of this property (Bishop, 1994; Prasad and Williams, 1991). As per the available literature numerous current studies display that besides a suitable action of electron correlation and a careful selection of the basis set function, the calculations of molecular electrical properties like polarizability and hyperpolarizability the inclusion of contributions arising from the nuclear motion is of fundamental importance (Ingamells et al., 1998; Raptis et al., 1999; Eckart et al., 2001).

Author know that the importance of the polarizability and first hyperpolarizability values of any molecule is reliant on the efficiency of electronic communication between acceptor and donor groups as these are the key elements in molecular charge transfer (Udayakumar et al., 2011; Wolinski et al., 1990; Cheeseman et al., 1996; Kalinowski et al., 1988; Pihlaja et al., 1994). To calculate the linear and nonlinear optical properties of LH2NB molecule author have applied B3LYP, CAM-B3LYP and wb97xd levels of theory using 6-31G** basis set. The calculated values of electronic dipole moment (μ), total average polarizability (α_{tot}), anisotropy of polarizability ($\Delta\alpha$), static first hyperpolarizability (β_0) and total first hyperpolarizability (β_{tot}) are presented in Table 7 at B3LYP/6-31G** level of theory. The above said values calculated by other methods are presented in Tables 8–10.
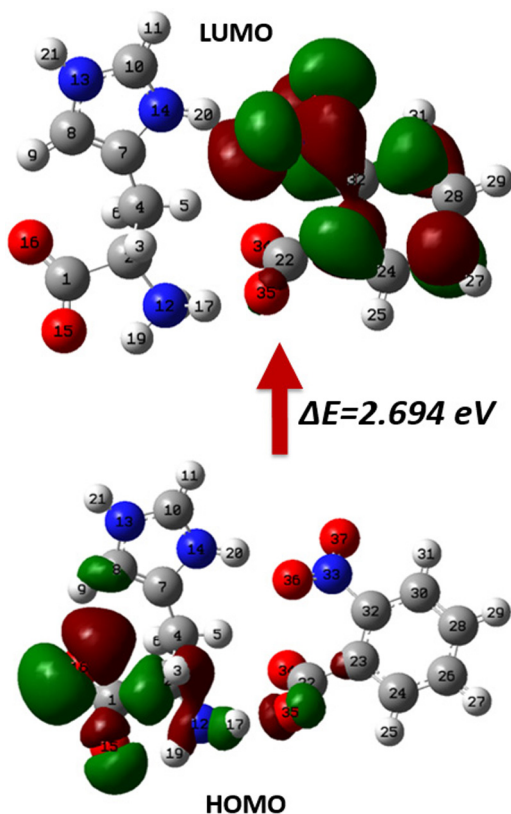
Figure 5   The 3-D plot of HOMO–LUMO orbitals of LH2NB molecule at isoval = ±0.02 a.u.
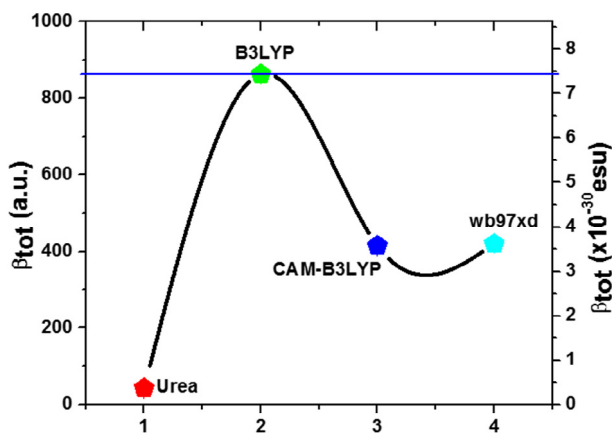

Figure 6   Variation of β_{tot} values calculated at different methods in comparison with urea.

The different mathematical expressions are used to calculate the above parameters as expressed below:

Total dipole moment is calculated by:

$$\mu_{tot} = \left(\mu_x^2 + \mu_y^2 + \mu_z^2 \right)^{\frac{1}{2}} \tag{9}$$

Total polarizability is calculated by:

$$\alpha_{tot} = \frac{1}{3} \left(\alpha_{xx} + \alpha_{yy} + \alpha_{zz} \right) \tag{10}$$

Table 6   The calculated energy values of frontier molecular orbitals (FMOs), energy difference and global reactivity descriptors at B3LYP/6-31G** level of theory.

Orbitals	B3LYP	
	a.u.	eV
E_{HOMO}	−0.200	−5.442
E_{HOMO-5}	−0.243	−6.612
E_{HOMO-1}	−0.211	−5.742
E_{LUMO}	−0.101	−2.748
E_{LUMO+1}	−0.058	−1.578
$\Delta E_{HOMO-LUMO}$	0.099	2.694
$\Delta E_{HOMO-5-LUMO}$	0.142	3.864
$\Delta E_{HOMO-1-LUMO+1}$	0.153	4.163
η	0.05	1.347
μ	−0.151	−4.095
s	0.074	2.020
χ	0.151	4.095
ω	0.229	6.225

Anisotropy of polarizability is calculated by:

$$\Delta\alpha = \frac{1}{\sqrt{2}}$$
$$\times \sqrt{\left[(\alpha_{xx} - \alpha_{yy})^2 + (\alpha_{yy} - \alpha_{zz})^2 + (\alpha_{zz} - \alpha_{xx})^2 + 6\alpha_{xz}^2 \right]} \tag{11}$$

The components of first hyperpolarizability can be calculated using the following relation:

$$\beta_i = \beta_{iii} + \sum_{i \neq j} \left[\frac{(\beta_{ijj} + 2\beta_{jii})}{3} \right] \tag{12}$$

Using x, y, z components the magnitude of first hyperpolarizability (β_{tot}) can be achieved by:

$$\beta_{tot} = \sqrt{(\beta_x^2 + \beta_y^2 + \beta_z^2)} \tag{13}$$

where β_x, β_y and β_z are:

$$\beta_x = (\beta_{xxx} + \beta_{xxy} + \beta_{xyy})$$
$$\beta_y = (\beta_{yyy} + \beta_{xxz} + \beta_{yyz})$$
$$\beta_z = (\beta_{xzz} + \beta_{yzz} + \beta_{zzz})$$

So, the final equation for magnitude of total first hyperpolarizability calculation is given by:

$$\beta_{tot} = \sqrt{\left[(\beta_{xxx} + \beta_{xxy} + \beta_{xyy})^2 + (\beta_{yyy} + \beta_{xxz} + \beta_{yyz})^2 + (\beta_{xzz} + \beta_{yzz} + \beta_{zzz})^2 \right]} \tag{14}$$

Table 7   Thermodynamic parameters of LH2NB molecule.

Methods	E (Thermal) (KCal/Mol)	C_V (Cal/Mol-Kelvin)	S (Cal/Mol-Kelvin)
HF	204.003	71.220	151.059
B3LYP	189.505	76.461	153.956
CAM-B3LYP	192.504	75.144	152.836
Wb97xd	192.562	74.984	149.904

Table 8 The calculated values of polarizability (α), dipole moment (μ) and hyperpolarizability (β) along their individual tensor components of LH2NB at B3LYP/6-31G** level of theory.

Components	a.u.	esu ($\times 10^{-24}$)	Component	a.u.	esu ($\times 10^{-30}$)
α_{xx}	247.415	36.667	β_{xxx}	26.530	0.229
α_{xy}	−4.757	−0.705	β_{xxy}	458.966	3.960
α_{yy}	205.029	30.385	β_{xyy}	29.511	0.255
α_{xz}	3.504	0.519	β_{yyy}	706.008	6.092
α_{yz}	−6.248	−0.926	β_{xxz}	−39.513	−0.341
α_{zz}	97.932	14.514	β_{xyz}	35.165	0.303
α_{tot}	183.459	27.189	β_{yyz}	24.906	0.215
$\Delta\alpha$	133.576	19.795	β_{xzz}	22.689	0.196
μ_x	1.296	−3.292D	β_{yzz}	22.695	0.196
μ_y	4.395	11.163D	β_{zzz}	−6.459	−0.056
μ_z	0.711	−1.805D	β_0	517.805	4.468
μ_{tot}	4.637	11.777D	β_{tot}	863.008	7.447
μ_{urea}	0.541	1.3732D (Govindarasu and Kavitha, 2014; Shkir and et al., 2015b)	β_{urea}	43.203	0.3728 (Govindarasu and Kavitha, 2014; Shkir and et al., 2015b)

Table 9 The calculated values of polarizability (α), hyperpolarizability (β) and dipole moment (μ) along their individual tensor components of LH2NB calculated at CAM-B3LYP/6-31G** level of theory.

Components	a.u.	esu ($\times 10^{-24}$)	Component	a.u.	esu ($\times 10^{-30}$)
α_{xx}	230.762	34.199	β_{xxx}	−140.742	−1.215
α_{xy}	−2.754	−0.408	β_{xxy}	211.661	1.826
α_{yy}	192.930	28.592	β_{xyy}	3.060	0.026
α_{xz}	3.726	0.552	β_{yyy}	421.943	3.64
α_{yz}	−7.240	−1.073	β_{xxz}	−40.938	−0.353
α_{zz}	100.936	14.958	β_{xyz}	28.431	0.245
α_{tot}	174.876	25.916	β_{yyz}	26.563	0.229
$\Delta\alpha$	115.993	17.19	β_{xzz}	16.941	0.146
μ_x	1.404	−3.329D	β_{yzz}	19.055	0.164
μ_y	4.462	11.058D	β_{zzz}	−8.906	−0.077
μ_z	0.820	−2.053D	β_0	249.067	2.149
μ_{tot}	4.749	11.730D	β_{tot}	415.112	3.582
μ_{urea}	0.541	1.3732D (Govindarasu and Kavitha, 2014; Shkir et al., 2015b)	β_{urea}	43.203	0.3728 (Govindarasu and Kavitha, 2014; Shkir et al., 2015b)

First hyperpolarizability can be labeled as a $3 \times 3 \times 3$ matrix as it is known as a third rank tensor and 27 components of the 3D matrix are reduced to 10 components due to the Kleinman symmetry (Kleinman, 1962), and can be specified in lower tetrahedral format as it is evident that the lower part of $3 \times 3 \times 3$ matrices is tetrahedral. Further, the static first hyperpolarizability (β_0) was also calculated using the following relation $\beta_0 = \frac{3}{5}\beta_{tot}$ and given in Table 7. The electronic communication of two different parts of any system plays a key role in polarizability and hyperpolarizability values. Calculated values of all components and their resultants of dipole moment, polarizability and hyperpolarizability by B3LYP/6-31G** are given in Table 7 (in a.u and esu (for α, 1 a.u. = 0.1482×10^{-24} esu and for β, 1 a.u. = 0.008629×10^{-30} esu)) (Govindarasu and Kavitha, 2014; Shkir et al., 2015b). The value of μ_{tot} and β_{tot} at molecular level are found to be 8 times and 20 times higher than urea ($\mu_{Urea} = 1.3732D$ and $\beta_{urea} = 0.3728 \times 10^{-30}$ esu) (Govindarasu and Kavitha, 2014; Shkir et al., 2015b) respectively. These values are higher than many other organic, semiorganic and inorganic materials also (Shkir et al., 2014, 2015b; Adant et al., 1995; Karabacak and 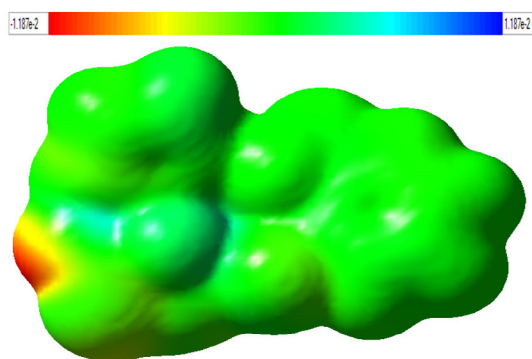Cinar, 2012; Raju et al., 2015; Abbas et al. 2015; Singh et al., 2012; Govindarasu et al., 2014). Further, these values were calculated by exchange correlation functional CAM-B3LYP and wb97xd level of theory with 6-31G** basis set and presented in Table 8 and 9. In recent reports the experimental value of second harmonic generation of LH2NB was found to be 2 times higher than KDP at bulk level (Moovendaran et al., 2013; Natarajan et al., 2012). The representation of variation of first order hyperpolarizability calculated at all the methods with reference to urea is shown in Fig. 6. Therefore, from both experimental and theoretical studies it is evident that the titled compound is a very good nonlinear optical material and can be useful for laser device applications.

3.6. Molecular electrostatic potential (MEP) analysis

Fig. 7 shows the MEP (3-D plot) of LH2NB molecule. MEP plays a very important role in understanding many points such as: (i). About its positive and negative regions as nucleophile and electrophile at molecular level(Murray and Sen, 1996; Scrocco and Tomasi, 1978), (ii). It is a measurement of electrostatic potential on constant electron density surface, (iii). It is

Table 10 The calculated values of polarizability (α), hyperpolarizability (β) and dipole moment (μ) along their individual tensor components of LH2NB calculated at wb97xd/6-31G** level of theory.

Components	a.u.	esu ($\times 10^{-24}$)	Component	a.u.	esu ($\times 10^{-30}$)
α_{xx}	233.588	34.618	β_{xxx}	−144.983	−1.251
α_{xy}	−3.531	−0.523	β_{xxy}	243.199	2.099
α_{yy}	194.649	28.847	β_{xyy}	−10.829	−0.093
α_{xz}	3.173	0.47	β_{yyy}	413.895	3.571
α_{yz}	−7.131	−1.057	β_{xxz}	−35.636	−0.307
α_{zz}	99.735	14.781	β_{xyz}	26.934	0.232
α_{tot}	175.991	26.082	β_{yyz}	31.685	0.273
$\Delta\alpha$	119.377	17.692	β_{xzz}	20.229	0.175
μ_x	1.354	−3.441D	β_{yzz}	18.165	0.156
μ_y	4.545	11.553D	β_{zzz}	−9.987	−0.086
μ_z	0.817	−2.076D	β_0	252.070	2.175
μ_{tot}	4.812	12.232D	β_{tot}	420.116	3.625
μ_{urea}	0.541	1.3732D (Govindarasu and Kavitha, 2014; Shkir and et al., 2015b)	β_{urea}	43.203	0.3728 (Govindarasu and Kavitha, 2014; Shkir and et al., 2015b)

Figure 7 MEP plot of LH2NB molecule at ISO value 0.02.

also a very useful property to examine the reactivity of molecular species by guessing that either the approaching nucleophile is attracted to a positive region of the molecular system (iv). It will also help to know the simultaneous information about the molecular size, shape along with its positive, negative and neutral electrostatic potential regions in terms of color grading (Murray and Sen, 1996; Lowdin, 1979). The MEP plot was also determined at HF/6-31G** level of theory and shown in Figure 3S (see supplementary data). The red and blue colors on surface shows highest negative and positive potential respectively.

The COO group of L-Histidine shows the negative potential as represented by red as well as yellow colors which is favorable for electrophilic attack while near the other atoms, it has positive potential with blue color and favorable for nucleophilic attack. The yellow color on the surface shows intermediate negative potential. The green color represents the slight positive or neutral potential over the carbon atoms.

4. Conclusions

The stable geometry of LH2NB molecule has been achieved and the optimized structural parameters were found in good agreement with the reported experimental values. The calculated vibrational modes of LH2NB are found in strong agreement with earlier experimental reports. The excitation energy of LH2NB molecule was calculated by TD-B3LYP, TD-CAM-B3LYP, TD-wb97xd, TD-PBE0 and TD-MO6 using 6-31G** basis set, and found to be 3.778, 4.012, 3.991, 3.935 and 3.820 eV and with an oscillatory strength of 0.045, 0.020, 0.023, 0.0377 and 0.0386 respectively. The charge interaction taking place within the molecule has been studied from HOMO–LUMO orbitals and energy gap was calculated. The chemical and thermal stability of LH2 NB has been studied with help of global chemical reactivity descriptors and thermodynamic parameters. The value of dipole moment is found to be lower in the excited state than ground state and shows that the ground state is more polar than excited state. The μ_{tot} and β_{tot} values are found to be 8 and 20 times higher than standard urea molecule at molecular level respectively. The molecular electrostatic potential plot shows that the negative potential sites are on electronegative oxygen atoms of COO group and positive potential sites are on hydrogen atoms. The higher total first hyperpolarizability indicates that the studied compound is maybe an excellent candidate for laser device applications.

Acknowledgement

Appendix A. Supplementary data

Supplementary data associated with this article can be found, in the online version, at http://dx.doi.org/10.1016/j.jksus.2016.03.002.

References

Abbas, H., Shkir, M., AlFaify, S., 2015. Density functional study of spectroscopy (IR), electronic structure, linear and nonlinear optical properties of L-proline lithium chloride and L-proline lithium bromide monohydrate: For laser applications. Arab. J. Chem. http://dx.doi.org/10.1016/j.arabjc.2015.02.011.

Adamo, C., Barone, V., 1999. Toward reliable density functional methods without adjustable parameters: the PBE0 model. J. Chem. Phys. 110 (13), 6158–6170.

Adant, C., Dupuis, M., Bredas, J., 1995. Ab initio study of the nonlinear optical properties of urea: electron correlation and dispersion effects. Int. J. Quantum Chem. 56 (S29), 497–507.

Ahmed, A.B. et al, 2008. Structural, vibrational and theoretical studies of l-histidine bromide. J. Mol. Struct. 888 (1), 180–186.

Alcolea Palafox, M., 2000. Scaling factors for the prediction of vibrational spectra. I. Benzene molecule. Int. J. Quantum Chem. 77 (3), 661–684.

Anandan, P., Jayavel, R., 2011. Crystal growth and characterization of semiorganic single crystals of L-histidine family for NLO applications. J. Cryst. Growth 322 (1), 69–73.

Arivazhagan, M., Meenakshi, R., 2012. Vibrational spectroscopic studies and DFT calculations of 4-bromo-o-xylene. Spectrochim. Acta Part A Mol. Biomol. Spectrosc. 91, 419–430.

Aruna, S. et al, 2007. Growth and characterization of semi organic nonlinear optical LHPCL crystals. Cryst. Res. Technol. 42 (2), 180–185.

Babu, G.A. et al, 2010. Synthesis, growth, structural, thermal, linear and nonlinear optical properties of a new organic crystal: dimethylammonium picrate. J. Cryst. Growth 312 (12), 1957–1962.

Becke, A.D., 1993. Density-functional thermochemistry. III. The role of exact exchange. J. Chem. Phys. 98, 5648–5652.

Bishop, D.M., 1994. Aspects of non-linear-optical calculations. Adv. Quantum Chem. 25, 1–45.

Boomadevi, S., Mittal, H., Dhansekaran, R., 2004. Synthesis, crystal growth and characterization of 3-methyl 4-nitropyridine 1-oxide (POM) single crystals. J. Cryst. Growth 261 (1), 55–62.

Chai, J.-D., Head-Gordon, M., 2008. Systematic optimization of long-range corrected hybrid density functionals. J. Chem. Phys. 128, 084106.

Cheeseman, J.R. et al, 1996. A comparison of models for calculating nuclear magnetic resonance shielding tensors. J. Chem. Phys. 104 (14), 5497–5509.

Chemla, D.S., 2012. In: Nonlinear Optical Properties of Organic Molecules and Crystals, vol. 1. Elsevier.

Cinar, M., Coruh, A., Karabacak, M., 2014. A comparative study of selected disperse azo dye derivatives based on spectroscopic (FT-IR, NMR and UV–Vis) and nonlinear optical behaviors. Spectrochim. Acta Part A Mol. Biomol. Spectrosc. 122, 682–689.

Cole, J.M., Howard, J.A., McIntyre, G.J., 2001. Influence of hydrogen bonding on the second harmonic generation effect: neutron diffraction study of 4-nitro-4'-methylbenzylidene aniline. Acta Crystallogr. B 57 (3), 410–414.

Colthup, N., 2012. Introduction to Infrared and Raman Spectroscopy. Elsevier.

Cossi, M., Barone, V., 2001. Time-dependent density functional theory for molecules in liquid solutions. J. Chem. Phys. 115 (10), 4708–4717.

Cuadrado, J.A. et al, 2000. Speciation of gold (III)–L-histidine complex: a multi-instrumental approach. This is the work of United States government employees engaged in their official duties. As such it is in the public domain and exempt from copyright.© US government. J. Environ. Monit. 2 (4), 355–359.

Dhanalakshmi, B., Ponnusamy, S., Muthamizhchelvan, C., 2010. Growth and characterization of a solution grown, new organic crystal: l-histidine-4-nitrophenolate 4-nitrophenol (LHPP). J. Cryst. Growth 313 (1), 30–36.

Dhas, S.M.B., Natarajan, S., 2008. Growth and characterization of two new NLO materials from the amino acid family: l-Histidine nitrate and l-Cysteine tartrate monohydrate. Opt. Commun. 281 (3), 457–462.

Dhas, S.M.B. et al, 2008. Growth and characterization of a new organic non-linear optical (NLO) material: L-histidinium trifluoroacetate. Open Crystal. J. 1, 46–50.

Dollish, F.R., Fateley, W.G., Bentley, F.F., 1974. Characteristic Raman Frequencies of Organic Compounds. Wiley.

Dreuw, A., Head-Gordon, M., 2004. Failure of time-dependent density functional theory for long-range charge-transfer excited

states: The Zincbacteriochlorin−Bacteriochlorin and Bacteri-ochlorophyll−Spheroidene complexes. J. Am. Chem. Soc. 126, 4007–4016.

Eckart, U. et al, 2001. Vibrational effects on electric properties of cyclopropenone and cyclopropenethione. J. Chem. Phys. 114 (2), 735–745.

Elleuch, S., Feki, H., Abid, Y., 2007. HF, MP2 and DFT calculations and spectroscopic study of the vibrational and conformational properties of N-diethylendiamine. Spectrochim. Acta Part A Mol. Biomol. Spectrosc. 68 (3), 942–947.

Fischer, E., Sterzel, H.J., Wegner, G., 1973. Investigation of the structure of solution grown crystals of lactide copolymers by means of chemical reactions. Kolloid-Zeitschrift und Zeitschrift für Polymere 251, 980–990.

Foster, M.E., Wong, B.M., 2012. Nonempirically tuned range-separated DFT accurately predicts both fundamental and excitation gaps in DNA and RNA nucleobases. J. Chem. Theory Comput. 8, 2682–2687.

Frisch, M.J., et al., Gaussian 09, Revision B.01. 2009, Wallingford CT.

Fujiwara, M. et al, 2006. Second order nonlinear optical properties of the single crystal of N-Benzyl 2-methyl-4-nitroaniline: Anomalous enhancement of the d333 component and its possible origin. Jpn. J. Appl. Phys. 45 (11R), 8676.

Gibbs, G.V., Crawford, T.D., Wallace, A.F., et al, 2011. Role of long-range intermolecular forces in the formation of inorganic nanoparticle clusters. J. Phys. Chem. A 115, 12933–12940.

Govindarajan, M. et al, 2011. Experimental (FT-IR and FT-Raman), electronic structure and DFT studies on 1-methoxynaphthalene. Spectrochim. Acta Part A Mol. Biomol. Spectrosc. 79 (3), 646–653.

Govindarasu, K., Kavitha, E., 2014. Vibrational spectra, molecular structure, NBO, UV, NMR, first order hyperpolarizability, analysis of 4-Methoxy-4′-Nitrobiphenyl by density functional theory. Spectrochim. Acta Part A Mol. Biomol. Spectrosc. 122, 130–141.

Govindarasu, K., Kavitha, E., Sundaraganesan, N., 2014. Synthesis, structural, spectral (FTIR, FT-Raman, UV, NMR), NBO and first order hyperpolarizability analysis of N-phenylbenzenesulfonamide by density functional theory. Spectrochim. Acta Part A Mol. Biomol. Spectrosc. 133, 417–431.

Ingamells, V.E. et al, 1998. The electronic, vibrational and rotational contributions to the dipole moment, polarizability, and first and second hyperpolarizabilities of the BH molecule. J. Chem. Phys. 109 (5), 1845–1859.

Jacquemin, D. et al, 2004. Theoretical investigation of substituted anthraquinone dyes. J. Chem. Phys. 121 (4), 1736–1743.

Jacquemin, D., Preat, J., Perpète, E.A., 2005. A TD-DFT study of the absorption spectra of fast dye salts. Chem. Phys. Lett. 410 (4), 254–259.

Johnson, B.G., Gill, P.M., Pople, J.A., 1993. The performance of a family of density functional methods. J. Chem. Phys. 98 (7), 5612–5626.

Kalinowski, H.-O., Berger, S., Braun, S., 1988. Carbon-13 NMR spectroscopy.

Karabacak, M., Cinar, M., 2012. FT-IR, FT-Raman, UV spectra and DFT calculations on monomeric and dimeric structure of 2-amino-5-bromobenzoic acid. Spectrochim. Acta Part A Mol. Biomol. Spectrosc. 86, 590–599.

Kleinman, D., 1962. Nonlinear dielectric polarization in optical media. Phys. Rev. 126 (6), 1977.

Klimm, D., 2014. Electronic materials with a wide band gap: recent developments. IUCrJ 1 (5), 281–290.

Koopmans, T., 1933. Ordering of wave functions and eigenenergies to the individual electrons of an atom. Physica 1 (1), 104–113.

Kostova, I., Amalanathan, M., Joe, I.H., 2010. Molecular first order hyperpolarizability and vibrational spectral investigation of Warfarin sodium. Chem. Phys. 378 (1), 88–102.

Kushwaha, S. et al, 2011. The effect of Cr3 + doping on the crystalline perfection and optical properties of zinc tris (thiourea) sulfate, a nonlinear optical material. J. Appl. Crystallogr. 44 (5), 1054–1061.

Kushwaha, S. et al, 2014. Au 9+ swift heavy ion irradiation of Zn [CS (NH 2) 2] 3 SO 4 crystal: crystalline perfection and optical properties. Nucl. Instrum. Methods Phys. Res., Sect. B 338, 1–7.

Ledoux, I. et al, 1987. Generation of high-peak-power tunable infrared femtosecond pulses in an organic crystal: application to time resolution of weak infrared signals. JOSA B 4 (6), 987–997.

Lee, C., Yang, W., Parr, R.G., 1988. Development of the Colle-Salvetti correlation-energy formula into a functional of the electron density. Phys. Rev. B 37, 785.

Lowdin, P.O., 1979. In: Advances in Quantum Chemistry, vol. 11. Academic Press.

Madhavan, J. et al, 2006. Growth and characterization of a novel NLO crystal l-histidine hydrofluoride dihydrate (LHHF). J. Cryst. Growth 293 (2), 409–414.

Madhavan, J. et al, 2007. Growth and characterization of L-histidine hydrochloride monohydrate single crystals. Cryst. Res. Technol. 42 (1), 59–64.

Madhavan, J. et al, 2007. Growth and characterization of a new nonlinear optical l-histidine acetate single crystals. Opt. Mater. 29 (9), 1211–1216.

Moovendaran, K. et al, 2012. Structural, vibrational and thermal studies of a new nonlinear optical material: l-Asparagine-l-tartaric acid. Spectrochim. Acta Part A Mol. Biomol. Spectrosc. 92, 388–391.

Moovendaran, K., Dhas, S.M.B., Natarajan, S., 2013. Growth and characterization of L-histidinium 2-nitrobenzoate single crystals: a new NLO material. Optik-Int. J. Light Electron Opt. 124 (17), 3117–3119.

Murray, J.S., Sen, K., 1996. In: Molecular Electrostatic Potentials: Concepts and Applications, vol. 3. Elsevier.

Natarajan, S. et al, 2012. Crystal structure of L-histidinium 2-nitrobenzoate. J. Amino Acids 2012.

Parr, R.G., Chattaraj, P.K., 1991. Principle of maximum hardness. J. Am. Chem. Soc. 113 (5), 1854–1855.

Parr, R.G., Pearson, R.G., 1983. Absolute hardness: companion parameter to absolute electronegativity. J. Am. Chem. Soc. 105 (26), 7512–7516.

Pearson, R.G., 1985. Absolute electronegativity and absolute hardness of Lewis acids and bases. J. Am. Chem. Soc. 107 (24), 6801–6806.

Pearson, R.G., 1987. Recent advances in the concept of hard and soft acids and bases. J. Chem. Edu. 64 (7), 561.

Pihlaja, K., Kleinpeter, E., 1994. Carbon-13 NMR Chemical Shifts in Structural and Stereochemical Analysis. VCH Publishers.

Prasad, P.N., Williams, D.J., 1991. Introduction to nonlinear optical effects in molecules and polymers. Wiley, New York.

Raju, R. et al, 2015. FT-IR, molecular structure, first order hyperpolarizability, MEP, HOMO and LUMO analysis and NBO analysis of 4-[(3-acetylphenyl) amino]-2-methylidene-4-oxobutanoic acid. Spectrochim. Acta Part A Mol. Biomol. Spectrosc. 134, 63–72.

Raptis, S., Papadopoulos, M.G., Sadlej, A., 1999. The correlation, relativistic, and vibrational contributions to the dipole moments, polarizabilities, and first and second hyperpolarizabilities of ZnS, CdS, and HgS. J. Chem. Phys. 111 (17), 7904–7915.

Rauk, A., 2001. Orbital Interaction Theory of Organic Chemistry, second ed. John Wiley & Sons, New York, 2001, 34.

Reshak, A., Khan, W., 2014. The density functional study of electronic structure, electronic charge density, linear and nonlinear optical properties of single crystal alpha-LiAlTe 2. J. Alloy. Compd. 592, 92–99.

Roeges, N.P., 1994. A Guide to the Complete Interpretation of Infrared Spectra of Organic Structures. Wiley.

Scrocco, E., Tomasi, J., 1978. In: Lowdin, P. (Ed.), . In: Advances in Quantum Chemistry, vol. 2. Academic Press, New York.

Shakir, M. et al, 2009. Characterization of ZnSe nanoparticles synthesized by microwave heating process. Solid State Commun. 149 (45), 2047–2049.

Shakir, M. et al, 2009. Ferroelectricity in glycine picrate: an astonishing observation in a centrosymmetric crystal. Appl. Phys. Lett. 95 (25), p. 252902–252902-3.

Shakir, M. et al, 2010. Enhancement of second harmonic generation, optical and dielectric properties in L-asparagine monohydrate single crystals due to an improvement in crystalline perfection by annealing. J. Appl. Crystallogr. 43 (3), 491–497.

Shkir, M., Abbas, H., 2014a. Physico chemical properties of l-asparagine l-tartaric acid single crystals: a new nonlinear optical material. Spectrochim. Acta Part A Mol. Biomol. Spectrosc. 118, 172–176.

Shkir, M., Abbas, H., 2014b. On the ground and excited state of glycine–glutaric acid: a new organic material. Spectrochim. Acta Part A Mol. Biomol. Spectrosc. 125, 453–457.

Shkir, M. et al, 2014. Optical spectroscopy, crystalline perfection, etching and mechanical studies on P-nitroaniline (PNA) single crystals. Opt. Mater. 36 (3), 675–681.

Shkir, M. et al, 2014. Experimental and theoretical studies on bis (glycine) lithium nitrate (BGLiN): a physico-chemical approach. J. Phys. Chem. Solids 75 (8), 959–965.

Shkir, M. et al, 2015. First principal studies of spectroscopic (IR and Raman, UV-visible), molecular structure, linear and nonlinear optical properties of L-arginine p-nitrobenzoate monohydrate (LANB): a new non-centrosymmetric material. Spectrochim. Acta Part A Mol. Biomol. Spectrosc. 147, 84–92.

Shkir, M. et al, 2015a. A dual approach to study the electro-optical properties of a noncentrosymmetric l-asparagine monohydrate. Spectrochim. Acta Part A Mol. Biomol. Spectrosc. 137, 432–441.

Shkir, M. et al, 2015b. A physico-chemical approach to study the experimental and theoretical properties of l-ornithine monohydrochloride: an organic nonlinear optical material. Mater. Chem. Phys. 155, 36–46.

Shkir, M., Muhammad, S., AlFaify, S., 2015c. Experimental and density functional theory (DFT): a dual approach to study the various important properties of monohydrated L-proline cadmium chloride for nonlinear optical applications. Spectrochim. Acta Part A Mol. Biomol. Spectrosc. 143, 128–135.

Shkir, M. et al, 2015d. An investigation on the key features of a D-π-A type novel chalcone derivative for opto-electronic applications. RSC Adv. 5 (106), 87320–87332.

Singh, R.N. et al, 2012. Molecular structure, heteronuclear resonance assisted hydrogen bond analysis, chemical reactivity and first hyperpolarizability of a novel ethyl-4-{[(2,4-dinitrophenyl)-hydrazono]-ethyl}-3,5-dimethyl-1H-pyrrole-2-carboxylate: a combined DFT and AIM approach. Spectrochim. Acta Part A Mol. Biomol. Spectrosc. 92, 295–304.

Sinha, P. et al, 2004. Harmonic vibrational frequencies: scaling factors for HF, B3LYP, and MP2 methods in combination with correlation consistent basis sets. J. Phys. Chem. A 108 (42), 9213–9217.

Smith, B.C., 1998. Infrared Spectral Interpretation: A Systematic Approach. CRC Press.

Socrates, G., 2004. Infrared and Raman Characteristic Group Frequencies: Tables and Charts. John Wiley & Sons.

Srinivasan, P. et al, 2006. Studies on the growth and characterization of l-asparaginium picrate (LASP) a novel nonlinear optical crystal. Cryst. Growth Des. 6 (7), 1663–1670.

Teimouri, A. et al, 2009. Experimental and CIS, TD-DFT, ab initio calculations of visible spectra and the vibrational frequencies of sulfonyl azide-azoic dyes. Spectrochim. Acta Part A Mol. Biomol. Spectrosc. 72 (2), 369–377.

Udayakumar, V. et al, 2011. Experimental (FT-IR, FT-Raman) and theoretical (HF and DFT) investigation and HOMO and LUMO analysis on the structure of p-fluoronitrobenzene. Spectrochim. Acta Part A Mol. Biomol. Spectrosc. 83 (1), 575–586.

Vektariene, A., Vektaris, G., Svoboda, J., 2009. A theoretical approach to the nucleophilic behavior of benzofused thieno [3, 2-b] furans using DFT and HF based reactivity descriptors. Arkivoc 7, 311–329.

Wolinski, K., Hinton, J.F., Pulay, P., 1990. Efficient implementation of the gauge-independent atomic orbital method for NMR chemical shift calculations. J. Am. Chem. Soc. 112 (23), 8251–8260.

Wong, B.M., Piacenza, M., Della Sala, F., 2009. Absorption and fluorescence properties of oligothiophene biomarkers from long-range-corrected time-dependent density functional theory. PCCP 11, 4498–4508.

Yanai, T., Tew, D.P., Handy, N.C., 2004. A new hybrid exchange–correlation functional using the Coulomb-attenuating method (CAM-B3LYP). Chem. Phys. Lett. 393, 51–57.

Zhao, Y., Truhlar, D.G., 2008. The M06 suite of density functionals for main group thermochemistry, thermochemical kinetics, non-covalent interactions, excited states, and transition elements: two new functionals and systematic testing of four M06-class functionals and 12 other functionals. Theoret. Chem. Acc. 120 (1–3), 215–241.

Zyss, J., Nicoud, J., Coquillay, M., 1984. Chirality and hydrogen bonding in molecular crystals for phase-matched second-harmonic generation: N-(4-nitrophenyl)-(L)-prolinol (NPP). J. Chem. Phys. 81 (9), 4160–4167.